SCIENTIFIC REPORTS

OPEN

SUBJECT AREAS:
NEURODEGENERATION
EXPERIMENTAL MODELS OF DISEASE

Received
20 August 2014

Accepted
14 November 2014

Published
2 December 2014

Correspondence and requests for materials should be addressed to V.S. (shahin@uni-muenster.de)

Unravelling crucial biomechanical resilience of myelinated peripheral nerve fibres provided by the Schwann cell basal lamina and PMP22

Gonzalo Rosso[1], Ivan Liashkovich[1], Burkhard Gess[2], Peter Young[2], Alejandra Kun[3] & Victor Shahin[1]

[1]Institute of Physiology II, WWU Münster, Robert-Koch-Straße 27b 48149 Münster, Germany, [2]Department of Sleep Medicine and Neuromuscular Disorders, Albert-Schweitzer Campus 1, Geb. A1, 48149 Münster, Germany, [3]Department of Proteins and Nucleic Acids, Instituto de Investigaciones Biológicas Clemente Estable, Montevideo, Uruguay.

There is an urgent need for the research of the close and enigmatic relationship between nerve biomechanics and the development of neuropathies. Here we present a research strategy based on the application atomic force and confocal microscopy for simultaneous nerve biomechanics and integrity investigations. Using wild-type and hereditary neuropathy mouse models, we reveal surprising mechanical protection of peripheral nerves. Myelinated peripheral wild-type fibres promptly and fully recover from acute enormous local mechanical compression while maintaining functional and structural integrity. The basal lamina which enwraps each myelinated fibre separately is identified as the major contributor to the striking fibre's resilience and integrity. In contrast, neuropathic fibres lacking the peripheral myelin protein 22 (PMP22), which is closely connected with several hereditary human neuropathies, fail to recover from light compression. Interestingly, the structural arrangement of the basal lamina of *Pmp22*$^{-/-}$ fibres is significantly altered compared to wild-type fibres. In conclusion, the basal lamina and PMP22 act in concert to contribute to a resilience and integrity of peripheral nerves at the single fibre level. Our findings and the presented technology set the stage for a comprehensive research of the links between nerve biomechanics and neuropathies.

The central nervous system (CNS) of the human body is naturally very well protected. The bones of the skull and the spinal column create a hard physical barrier which protects the CNS from injury. The peripheral nervous system (PNS), however, is considered to be rather vulnerable to mechanical stresses particularly to compression. On the other hand, the PNS is regularly exposed to mechanical compression related to function and participation in normal daily activities. In the PNS, every individual nerve fibre is wrapped in a protective sheath known as the endoneurium. The fibres are bundled together into groups known as fascicles, and each fascicle is surrounded by a protective sheath known as the perineurium. Several fascicles in turn are joined together with a blood supply and fatty tissue within yet another sheath, the epineurium. Peripheral nerves are thus supported by three layers of connective tissues. Unlike oligodendrocytes and their associated axons in the CNS, Schwann cells and axons in the PNS are enwrapped in a continuous basal lamina. The fairly thin basal lamina is mainly secreted by Schwann cells[1]. Different roles have been proposed for the basal lamina including Schwann cell proliferation, survival, migration, myelination, and formation of Ranvier nodes[2–4]. In addition, as an extracellular matrix the basal lamina is likely to contribute to the structural support of peripheral nerves but it remains unknown whether it also contributes to their mechanical support. There seem to be close links between vulnerability of peripheral nerves to mechanical compression and various neuropathies[5]. Nonetheless, the links remain barely understood so far. Moreover, the possibility should be considered that impaired biomechanics of peripheral nerves may result from impaired biomechanics of the individual nerve fibres within the nerve. Hence, there is an urgent need for appropriate research strategy and technology enabling biomechanical and integrity investigations on individual nerve fibres. Here we report the use of a research strategy based on the application of advanced technology. We simultaneously combine atomic force and confocal scanning microscopy for simultaneous biomechanical and integrity investigations on individual and viable nerve fibres. Given the absence of a hard protective physical barrier around peripheral nerves, our hypothesis is as follows: Inherent structural elements of peripheral nerves

intrinsically impart biomechanical resilience and integrity to nerves, which is critical to their function. Consequently, impaired biomechanics of peripheral nerves should have direct implications for peripheral neuropathies. We test this hypothesis on isolated nerve fibres from wild-type and hereditary neuropathy mouse models lacking the peripheral myelin protein-22 (PMP22). PMP22 has been suggested to play a role in proliferation, differentiation, and death of Schwann cells[6–8]. It is also well-known to be crucially involved in numerous hereditary peripheral neuropathies including Charcot-Marie-Tooth disease[5,9–11] and the hereditary neuropathy with liability to pressure palsies (HNPP)[12]. However, the exact biological role of PMP22 remains barely understood. In addition, PMP22 has recently been suggested to provide mechanical support to nerves[13] and nerve fibres[14]. Nonetheless, the mechanisms underlying the links between PMP22, mechanical support of peripheral nerves and neuropathies remain unclear so far.

Results

Designing a strategy for simultaneous biomechanical, structural and functional integrity investigations on isolated viable myelinated peripheral nerve fibres. Myelinated peripheral nerve fibres are obtained from 90–120 days old adult mice as described in Methods. To verify that the isolated fibres remain viable in their neurobasal medium throughout the entire time of investigation at 37°C, we use a 5-bromouridine (BrU) assay[15]. BrU diffuses into the nucleus and incorporates specifically into newly-synthesised RNA. Using this method, we demonstrate that isolated nerve fibres remain viable for at least 4 hours at 37°C in the neurobasal medium (supplementary figure 2). Having verified that the nerve fibres remain viable for a sufficient period of time, we set out to perform the experiments according to a designed strategy. We use a setup combining AFM and confocal microscopy simultaneously. The setup enables us to study biomechanical properties, structural and functional integrity of the isolated myelinated nerve fibres simultaneously. Fibres are labelled with a specific myelin marker (red, supplementary figure 1) and kept in a neurobasal medium at 37°C during the entire time of investigation. The medium contains green fluorescent 70 kDa FITC-dextran, which serves two purposes: On one hand it allows the visualisation of the non-fluorescent AFM tip without labelling it such that a negative image of the AFM tip is obtained (supplementary figure 1). The tip can then be positioned very precisely over a selected region on the surface of the nerve fibre. Eventually, the biomechanical measurements are performed on the region as seen in figure 1. On the other hand, dextran remains naturally excluded from the interior of the nerve fibres as long as they are intact and viable. In other words, a loss of biomechanical, structural and functional integrity of the nerve fibres will be paralleled by dextran leakage into the interior of the fibres. The structural integrity is detected with both confocal microscopy and AFM. While the former provides information on the overall structural integrity, the latter enables structural investigation of the surface of the nerve fibres at the nano-scale.

Relationship between stiffness and diameter of adult myelinated peripheral nerve fibres. Figure 1 depicts real time biomechanical experiments (stiffness) on small, medium and large calibre fibres. Basically, the AFM allows the investigation of the stiffness of the nerve fibres as it compresses them mechanically with a nano-scale tip. At the same time, the confocal microscope provides high-resolution fluorescent images containing information about the nerve fibre deformation. The deformation of three different diameter nerve fibres is investigated by applying three increasing loading forces of 25 nN, 50 nN and 75 nN. At first glance, the large calibre fibre (fig. 1, top row) is assumingly less deformed than the medium (fig. 1, center row) and small calibre fibres (fig. 1, bottom row) at the same loading forces. In other words, the

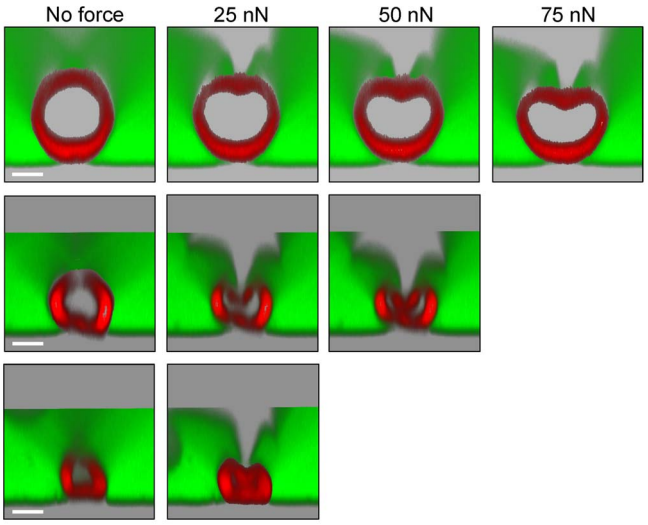

Figure 1 | Simultaneous combination of AFM and confocal microscopy for mechanical measurements on individual peripheral nerve fibres. Transverse confocal section images showing three different calibre fibres labelled with a specific myelin marker (red) and kept in neuronal medium containing 70 kDa FITC-dextran (green). A non-fluorescent pyramidal AFM tip (visualised as a grey shadow) applies incremental loading forces to gradually compress the nerve fibres in order to investigate their mechanical behavior. 6 small, 6 medium and 6 large calibre fibres were tested. Scale = 5 μm.

assumption may be made that the stiffness of the fibres depends on their diameters. However, a detailed analysis is necessary to either corroborate or discard this assumption. In order to find out if the stiffness of adult myelinated peripheral nerve fibres correlates with its diameter, the following experiment was designed as presented in figure 2. The AFM tip is placed 15 μm away from the surface (starting point) (fig. 2A). In the next step the tip is driven down to probe the glass surface mechanically and a corresponding force-indentation curve is recorded. The tip is then lifted off again to repeat the same cycle and probe the large (fig. 2C) and small (fig. 2D) calibre fibres mechanically one after the other. In all three cases, the AFM tip applies a preset loading force of 50 nN to probe the glass and the fibres. Both the outer diameters of the fibres as well as the extent of their indentation can be determined precisely from this experiment. The diameters of the large and small fibres are 8 μm and 4.5 μm, respectively (15 μm − 7 μm = 8 μm; 15 μm − 10.5 μm = 4.5 μm). The loading force of 50 nN indents both fibres to the same extent. Six fibres were tested in each condition. Mean stiffness values ± SEM are 53 ± 6.2 pN/nm and 51 ± 7.1 pN/nm for large and small calibre fibres, respectively. Accordingly, we conclude that the stiffness of the peripheral nerve fibres does not depend on their diameters.

Biomechanical resilience and integrity of adult myelinated peripheral nerve fibres. Having found out that the stiffness of the adult myelinated peripheral nerve fibre does not depend on its diameter, we set out to study the biomechanical properties and integrity of the fibres in more detail. After all, despite substantial indentation and structural changes imposed upon the fibres they do not seem to be damaged judging from the observations made so far. Mechanical resilience and structural integrity of large and small calibre peripheral myelinated nerve fibres are investigated both upon exposure to three incremental loading forces as well as after removal of the force. Thus, the response of nerve fibres to incremental mechanical compression is used as one of the measures for a mechanical resilience. As seen in figure 3, before exposure to force the fibres assume a rather circular shape as observed in the transverse

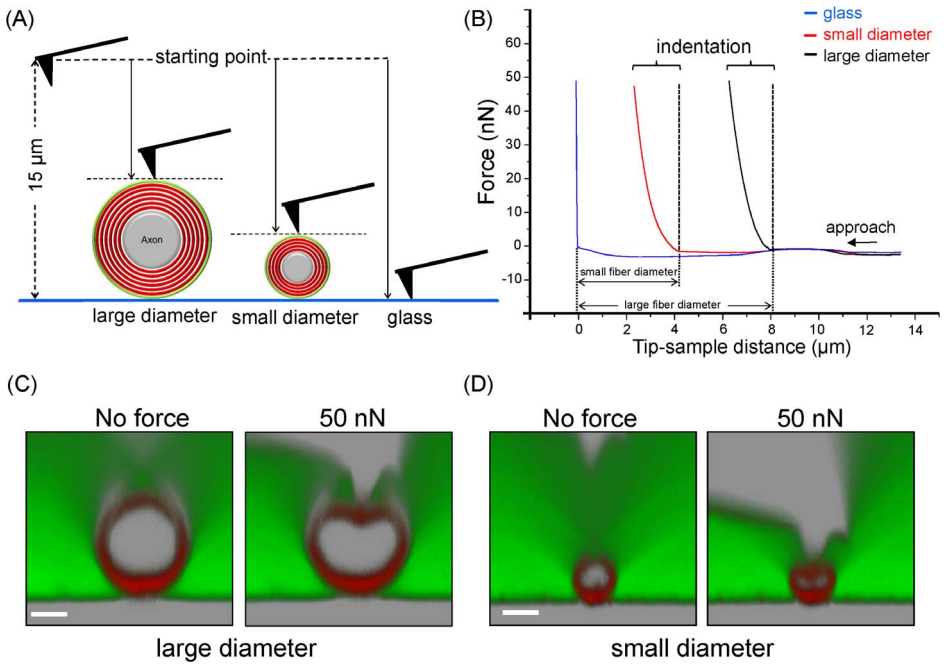

Figure 2 | Relationship between stiffness and diameter of peripheral nerve fibres. (A) Schematic of the experimental strategy designed to measure the stiffness of large and small diameter nerve fibres. Large and small diameter nerve fibres as well as glass are indented by the AFM tip at a preset loading force of 50 nN. The fibres are indented to the same extent at the same loading force regardless of their diameter. Force-indentation curves recorded for each condition are displayed in (B). 6 fibres were tested in each condition. Confocal microscopy images showing the corresponding nerve compression are shown in (C) and (D). Scale bars = 5 µm.

sections obtained with confocal microscopy. However, upon exposure of the fibres to loading forces of 25 nN, 50 nN and 75 nN they are compressed gradually. Compression is paralleled by a change of their structure. The large calibre fibre responds to increasing loading forces with a significant compression which is greatest at 75 nN. At the same force the small calibre fibre is even squeezed together. Since both fibres have the same stiffness but differ strongly in their diameter, the large calibre fibre will need forces significantly larger than 75 nN to be squeezed together. Remarkably, upon removal of the loading forces both fibres fully and promptlyrestore their original shape. The recovery time of 10 tested fibers ranged between 2 and 6 seconds.

Equally remarkable is the fact that dextran remains excluded from the fibres in all conditions. In other words, even when the fibres are squeezed together, they maintain their mechanical and structural integrity. The hard and sharp AFM tip exerts a substantial point pressure on the surface of the fibres and yet fails to induce any ruptures in the fibres which would otherwise be paralleled by dextran leakage into the fibres.

Contribution of the cytoskeleton, basal lamina and myelin to the biomechanical resilience and integrity of adult peripheral nerve fibres. AFM-based compression experiments were carried out on wild-type peripheral nerve fibres after specific disruption of the cytoskeleton with cytochalasin-D. Surprisingly, the overall mechanical properties of the fibres barely changed. In order to study the contribution of the basal lamina and myelin to the biomechanics and integrity of adult peripheral nerve fibres we treated the fibres with a collagenase which digests the basal lamina highly specifically while leaving the myelin intact. Samples were then imaged with AFM in liquid condition prior to biomechanical and integrity investigations. Figure 4 (A and B) shows topographical

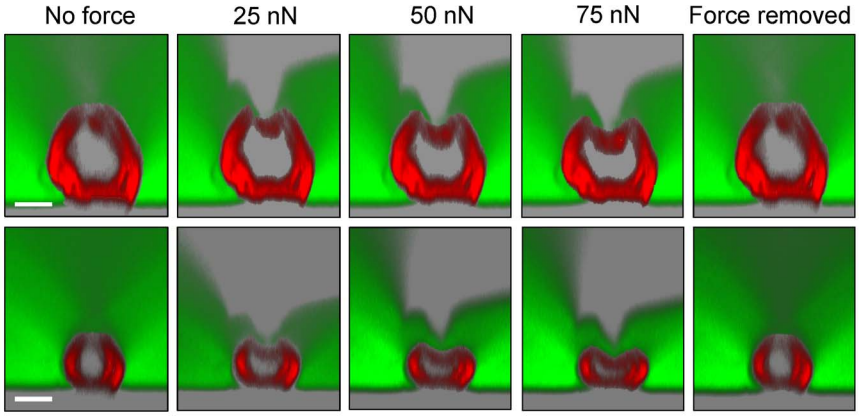

Figure 3 | Biomechanical and structural integrity of peripheral nerve fibres. Biomechanical resilience and structural integrity of large (top row) and small (bottom row) calibre peripheral nerve fibres are tested at increasing compression forces. Number of fibres is 6 each. Removal of the applied force results in full recovery of the fibres. Dextran remains excluded from the interior of the nerve fibres in all conditions. Scale bars = 5 µm.

AFM images of isolated peripheral nerve fibres before and after collagenase treatment, respectively. The basal lamina of untreated peripheral nerve fibres reveals interlaced type IV collagen fibres with a characteristic pattern (fig. 4A). Upon collagenase treatment, however, the basal lamina-stripped surface of Schwann cells becomes rather smooth (fig. 4B). Next, the response of nerve fibres to mechanical compression and their integrity with and without basal lamina were investigated with AFM and confocal microscopy. Untreated nerve fibres again fully and promptly recover from mechanical compression and maintain their integrity (fig. 4C,E). The force-indentation curve in figure 4E corresponds to the untreated nerve fibre in figure 4C and demonstrates its elastic behavior. In contrast, the basal lamina-stripped nerve fibre with intact myelin visibly loses its integrity resulting in massive dextran leakage into the axon (fig. 4D). Moreover, it is deprived of its biomechanical resilience which is demonstrated by the loss of its ability to recover from mechanical compression (fig. 4D). The corresponding force-indentation curve (fig. 4F) displays a characteristic 'breakthrough event' (mean breakthrough force ± SEM is 12.5 ± 5.4 nN, n = 11 fibres). This demonstrates significant disruption, softening and destabilisation of the nerve fibre following removal of the basal lamina. The above observations are repeatedly made on myelinated nerve fibres deprived of their basal lamina following collagenase treatment.

***Pmp22*$^{-/-}$ nerve fibres are characterised by vulnerability to mechanical compression, impaired integrity and significantly altered structural organisation of the basal lamina.** The homozygous *Pmp22*$^{-/-}$ mouse represents a valuable animal model to study the role of PMP22 and its relationship with the pathogenesis of hereditary peripheral neuropathies[16,17]. Here, we use this animal model to investigate and understand the potential contribution of PMP22 to the biomechanical resilience and integrity of peripheral nerve. Confocal microscopy images in figure 5 show transverse cross-sections of wild-type (top row) and *Pmp22*$^{-/-}$ (bottom row) nerve fibres during and after mechanical compression. Both types of fibres have in common the exclusion of dextran. Apart from this, they differ remarkably. The absence of PMP22 deprives nerve fibres from their elastic behavior (fig. 5A, bottom row). They recover only partially upon relief from compression when compared to wild-type fibres. In addition, *Pmp22*$^{-/-}$ nerve fibres sustain irreversible substantial structural damage following compression. Analysis of

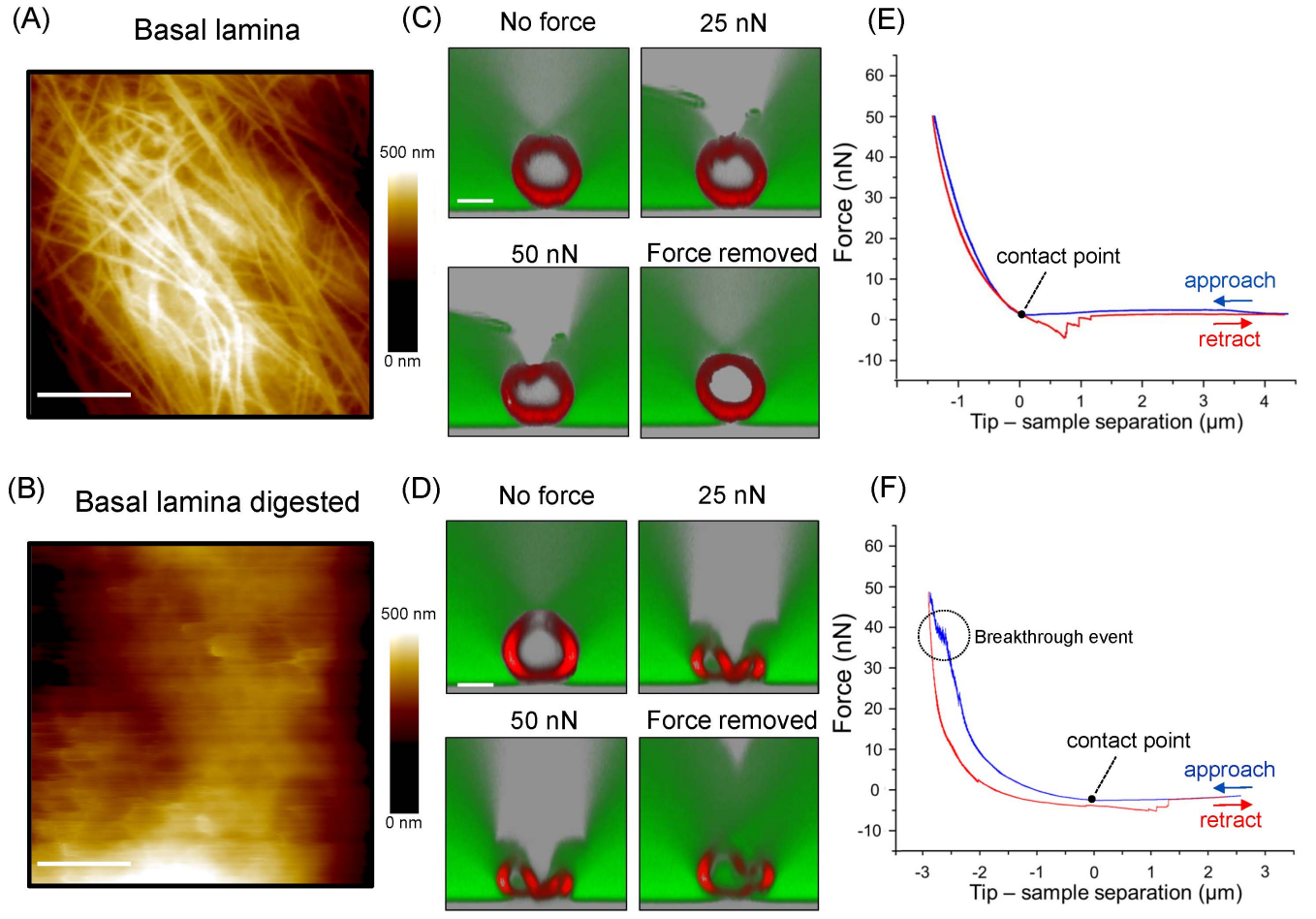

Figure 4 | The Schwann cell basal lamina accounts for the mechanical properties of peripheral nerve fibres. (A,C,E) and (B,D,F) show control and basal lamina-stripped nerve fibres, respectively. Representative topographical AFM images of myelinated nerve fibres before (A) and after (B) treatment with collagenase. Eleven fibres were tested in each condition. Digestion of Schwann cell basal lamina leads to a significant softening of the nerve fibre. This follows directly from the corresponding force-indentation curve (shallow slope in the approach curve compared to the slope in the approach curve of the untreated fibre). Softening is paralleled by high vulnerability to mechanical stress. Fibres fail to fully recover from mechanical compression. In addition, upon compression they lose their integrity which results in dextran leakage into the interior of the fibre ((D), arrow (insert arrow pointing to the dextran leak). (E) and (F) show single force curves obtained on untreated and basal lamina-stripped nerve fibres, respectively. Mechanical measurements on basal lamina-stripped nerve fibres are characterised by the presence of several so-called 'breakthrough' events (F) (Average breakthrough force ± SEM is12.5 ± 5.4 nN, n = 11 fibres). The latter result from mechanical disruption of the surface of the nerve fibre. Scales in (A,B) and (C,D) are 1 μm and 5 μm, respectively.

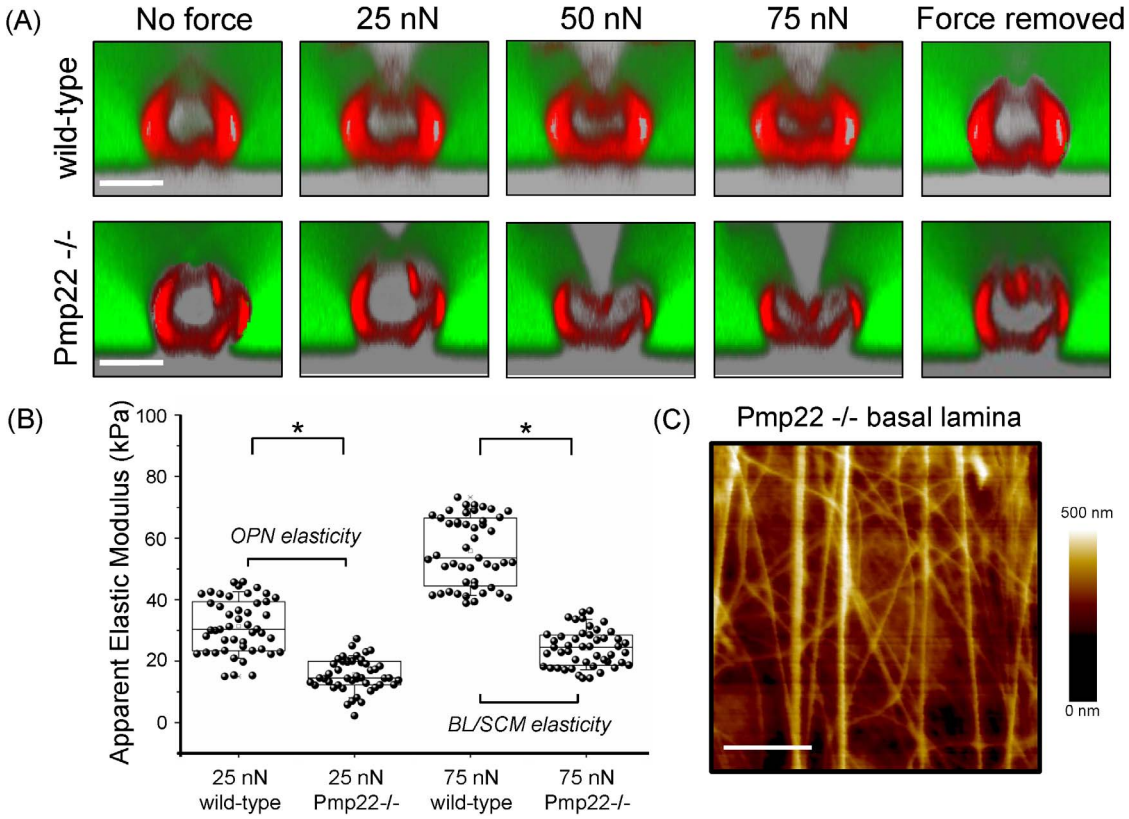

Figure 5 | Impaired nerve mechanics in *Pmp22*$^{-/-}$ peripheral nerve fibres. (A) Absence of PMP22 (compact myelin constituent) leads to structural and mechanical impairment in PMP22-null nerve fibres. *Pmp22*$^{-/-}$ nerve fibres fail to fully recover upon relief from mechanical compression. Graph in (B) shows OPN and BL/SCM elasticity values (estimated Young's modulus) obtained for wild-type (N = 4, n = 8) and *Pmp22*$^{-/-}$ nerve fibres (N = 3, n = 7) at 25 nN and 75 nN, respectively. N = number of animals, n = number of fibres. (C) *Pmp22*$^{-/-}$ nerve fibres show basal lamina impairment. The data in plot is shown as box-and-whiskers plot representing the median values. The borders of the boxes represent the 25% and 75% percentiles and a whisker range of 10–90. Scale in are 5 μm and 1 μm in A and C, respectively. (* $p < 0.05$).

the elasticity of nerve fibres as described in Methods and supplementary figure 3 reveals further remarkable differences between wild-type and *Pmp22*$^{-/-}$ nerve fibres. We distinguish between the overall peripheral nerve fibre (OPN) elasticity and that of the combination of the basal lamina (BL) and Schwann cell myelin (SCM). Figure 5B demonstrates a significant reduction in OPN and BL/SCM elasticity in *Pmp22*$^{-/-}$ in comparison with wild-type nerve fibres. The OPN elasticity at 25 nN for wild-type and *Pmp22*$^{-/-}$ are 31.4 ± 8.8 kPa and 15.6 ± 5.2 kPa, respectively. The BL/SCM elasticity drops significantly from 55.8 ± 11.1 kPa in wild-type nerve fibres to 24.2 ± 6.3 kPa in *Pmp22*$^{-/-}$. In addition, *Pmp22*$^{-/-}$ nerve fibres reveal a significantly altered basal lamina compared with wild-type fibres. Wild-type nerve fibres possess a dense and tight basal lamina with regularly interlaced fibrils forming a meshwork (fig. 4A). In contrast, *Pmp22*$^{-/-}$ nerve fibres show a loose and apparently less dense basal lamina with a parallel orientation pattern of its fibrils (fig. 5C).

Discussion

So far, several mechanical and structural investigations have been carried out on nerves but rarely on individual nerve fibres which make up the nerve. Heredia et al.[18] teased individual nerve fibres from the nerve, air-dried, froze and then rehydrated them before they eventually investigated their elasticity with AFM. Despite interesting new insights gained, the observations made do not remain without reservation with respect to the harsh treatments prior to investigation. In another publication, we investigated with AFM teased nerve fibres after fixation[14]. Bearing in mind that fixation affects the biomechanical properties of biological samples, our focus then was not on the biomechanics of nerve fibres. Besides, simultaneous biomechanical, structural and functional integrity investigations were not possible. Recently, AFM was applied to study biomechanical properties of axons during different myelination stages[19]. For this purpose, Schwann cells, co-cultured *in vitro* with PC12 cells for various times, were differentiated to form a myelinated axon. The resulting samples were then exposed to fixation prior to biomechanical investigation with AFM[19]. The conclusion was drawn that the biomechanical properties of the myelinating axons depended on the varying thickness and characteristics of the myelin sheath along the myelination stages[19]. Here, we carry out the investigations on myelinated axons using nerve fibres from adult wild-type mice. Besides, the fibres are not exposed to fixation and are thus viable during the entire investigation. We show that the overall stiffness of adult myelinated peripheral nerve fibres of different calibres is the same. It depends neither on the thickness of myelin nor on the diameter of the axon. We can imagine that during the myelination process the thickness of myelin affects the biomechanical properties of the axons. Once myelination is completed, however, myelin does not alter the overall biomechanical propertiesof the axons significantly. The adult myelinated peripheral nerve fibres tested in the present study withstand remarkable mechanical compression reversibly and without apparent damage or loss of integrity. Loading forces as high as 75 nN compress the fibres substantially and yet fail to disrupt their structural and functional integrity visibly. This is surprising considering the fact that the local loading force is exerted by a fairly sharp and hard AFM tip. Biological samples usually sustain visible structural damages at far lower loading forces. Even particularly rigid and highly dense biological samples with formidable

biomechanical and structural integrity, such as herpes simplex virus capsids, are not able to tolerate forces approaching 7 nN[20]. Based on our observations, it is obvious that the resilience of peripheral nerve fibres must come from their intrinsic structural elements. The most likely elements are naturally the thick myelin and/or the cytoskeleton. Surprisingly, specific disruption of the cytoskeleton with cytochalasin-D did not influence the biomechanical resilience and intergrity of adult myelinated wild-type nerve fibres. To study the potential contribution of myelin to the demonstrated biomechanical resilience and integrity of adult wild-type nerve fibres, we designed an experiment in which the AFM tip could compress myelin directly following specific removal of the basal lamina. Compression of myelinated basal lamina-stripped nerve fibres resulted in irreversible deformation of the fibres paralleled by abnormal and excessive leakage to large macromolecules (70 kDa dextran). Myelin tightness and its natural ability to fully exclude 70 kDa dextran have been recently demonstrated in peripheral nerve fibres from wild-type mice[21]. On the other hand, myelin rendered abnormally permeable to 70 kDa dextran in nerve fibres from *Pmp22*$^{+/-}$ mice[21], an animal model for the human hereditary neuropathy with liability to pressure palsies (HNPP). Leakage to 70 kDa dextran was only observed in the paranodal non-compact myelin regions[21]. In the present study, however, we observe excessive leakage to 70 kDa dextran through all compact and non-compact myelin regions of the mechanically compressed basal lamina-stripped peripheral nerve fibres from wild-type mice. The outcome of this experiment unravels that the basal lamina is the major contributor to biomechanical resilience, structural and functional integrity of the myelinated peripheral fibres. Moreover, the basal lamina might contribute to the tightening of the myelin. The basal lamina has been shown to interact with integrins in Schwann cells[22], and we can imagine that this interaction could further support the contribution of PMP22 to the tightening of myelin[21]. We recently studied the involvement of PMP22 in Charcot–Marie–Tooth type 1A, the most frequent human hereditary demyelinating neuropathy, using Trembler-J mice (Tr-J, missense mutation in PMP22 gene) as an animal model. Our findings implied a potential contribution of PMP22 to the mechanical support of demyelinated peripheral nerve fibres and a possible implication of the cytoskeleton was considered[14]. In another recent work discussed above using *Pmp22*$^{+/-}$ mice it could be demonstrated that PMP22 is crucial for the sealing, tightening and stabilisation of myelin through its involvement in the assembly of myelin junctions (such as tight junctions and adherens)[21]. Moreover, myelinated peripheral nerve fibres from the same animal model were found to be highly susceptible to mechanical compression thereby resulting in conduction block (CB)[13]. Hence, CB in *Pmp22*$^{+/-}$ nerves was concluded to result from the loss of myelin tightness and the susceptibility to mechanical compression[21]. In other words, two closely interconnected biological functions of PMP22 must be sealing/stabilisation of myelin and protection from nerve injury[13]. The highest levels of PMP22 are produced by myelinating Schwann cells. Two of the biological roles of PMP22 have been discussed above. Versatile other roles of PMP22 in the peripheral nerve remain unresolved. The potential roles of PMP22 were studied previously after engineering a novel knock-out (−/−) mouse line[22]. It could be demonstrated that in the absence of PMP22, myelination of peripheral nerves is delayed. In addition, numerous axon-Schwann cell profiles showed loose basal lamina, suggesting altered interactions of the glial cells with the extracellular matrix. The levels of beta4 integrin, a molecule involved in the linkage between Schwann cells and the basal lamina, were severely reduced in nerves of PMP22-deficient mice[22]. Together, these data indicate that PMP22 is a binding partner in myelin junctions, integrin/laminin complexes and is involved in mediating the interaction of Schwann cells with the extracellular environment[22]. In the present work we study the potential contribution of PMP22 to the biomechanical properties and integrity of peripheral nerves at the single nerve fibre level. We also address the relationship between PMP22 and the basal lamina. The observed alteration in the structural arrangement of the basal lamina in absence of PMP22 is accompanied by a high susceptibility of the myelinated peripheral nerve fibres to mechanical compression (fig. 5). Moreover, compression of *Pmp22*$^{-/-}$ nerve fibres inflicts significant irreversible structural deformation upon them. In addition, they are no longer able to fully restore their original shape upon relief from compression. Nevertheless, *Pmp22*$^{-/-}$ nerve fibres are still able to exclude 70-kDa FITC-dextran from the compact myelin regions. The permeability of myelin to 70 kDa dextran in the paranodal regions as convincingly demonstrated in *Pmp22*$^{+/-}$ peripheral nerve fibres[21] was irrelevant in the present study, and we can imagine that it will further increase in *Pmp22*$^{-/-}$ fibres.

Conclusions, physiological and pathophysiological relevance

Impairment in the basal lamina and/or PMP22 have direct implications for nerve dysfunction and neuropathies. The exact mechanisms underlying the interplay between the basal lamina and PMP22 remain to be investigated yet. Potential mechanisms, physiological and pathophysiological relevance may be as follows: Through interactions with integrins[22,23] and myelin junctions[21], PMP22 might strengthen the bonds between the basal lamina and the Schwann cells. This in turn might result in a tight pulling of the basal lamina onto the Schwann cells and eventually in an overall mechanical reinforcement of the entire nerve fibre. It is conceivable that a further mechanism of PMP22 action may be based on indirect beneficial intervention in the structural arrangement of the basal lamina thereby further reinforcing its protective role. Myelin may add up to the protective action of the basal lamina by acting as a shock absorbance under mechanical stresses. The well-known role of myelin is to ensure the physiologically crucial high conduction velocity of the myelinated nerve fibres. High conduction velocity requires thick, tight and electrically insulating myelin. Velocity also increases with increasing internal diameter of the myelinated axon. Based on our data, it is conceivable that the basal lamina and PMP22 may help ensure the high conduction velocity of myelinated peripheral nerve fibres in multiple ways. By providing biomechanical resilience and structural integrity they may reinforce the tightness of the myelin. At the same time they may increase the resistance of the thick myelin to compression. By enabling the myelinated nerve fibre to recover promptly from acute compression, they may prevent a prolonged constriction of the axon. In addition to the discussed potential role in conduction velocity we can imagine the biomechanical resilience of myelinated nerve fibres to play another physiological role. Their ability to recover fast from mechanical compression is not only essential to ensure their high conduction velocity but may also provide a mechanical support to the entire nerve. This would on one hand increase the resistance of the nerve to compression and on the other hand help the nerve to recover promptly upon relief. This in turn would ensure the crucial blood flow within the nerve which is highly sensitive to ischemia.

Methods

Isolation and preparation of adult myelinated peripheral nerve fibres. Animal studies and procedures were conducted in accordance with the European Convention for Animal Care and Ethical Use of Laboratory Animals and have been approved by the local governmental authorities (State Office for Nature, Environment and Consumer Protection, North Rhine-Westphalia, Germany; File reference 84-02.05.20.12.146). Animals were maintained in standard laboratory conditions with a 12 h/12 h light-dark cycle and allowed free access to food and water. The number of animals was kept to a minimum needed. Animals were euthanised by isofluoran overdose and cervical dislocation. Peripheral nerve fibres were obtained from 90–120 days old C57BL/6 wild-type and homozygous *Pmp22*$^{-/-}$ adult mice (assayed by molecular genotyping). Briefly, an incision was made at mid-thigh and both sciatic nerves (1-cm segment) were harvested and immediately immersed in ice-cold Neurobasal medium (Invitrogen, CA, USA). Then, nerve fibres were released from epineurium using #5 forceps and thoroughly mechanically separated and teased over glass cover slips pretreated Cell-Tak™ (BD Biosciences, CA, USA). Immediately after

teasing, nerve fibres were incubated in 400 µl Neurobasal medium (Invitrogen, CA, USA) containing FluoroMyelin™ Red (Invitrogen, CA, USA; 1 : 250) for Schwann cell myelin staining and placed in incubator for 30 minutes at 37°C with 5% atmospheric CO_2. FlouroMyelin™ Red is a commercial available water-soluble fluorescent dye with selectivity staining for myelin sheaths and has a proven photo-stability for live imaging of myelin showing no apparent toxicity and adverse effects on myelin sheaths or axons[24]. Finally, medium containing FluoroMyelin™ Red was replaced with 37°C pre-heated Neurobasal medium containing 1 mg/ml 70 kDa FITC-dextran (Sigma-Aldrich, MO, USA). For Schwann cell basal lamina disruption experiments, isolated nerve fibres were incubated for 20 minutes at 37°C in Neurobasal medium containing 0.05% (w/v) of CLSPA collagenase enzyme (Whortington, NJ, USA) - kindly provided by Dr. Uwe Hensen (Institute of Physiological Chemistry and Pathobiochemistry, University of Münster). After treatment, nerve fibres were washed with Neurobasal medium and prepared for mechanical measurements as described above. AFM images of Schwann cell basal lamina were performed on 3% paraformaldehyde fixed nerve fibres in contact mode under liquid conditions.

Testing the viability of nerve fibres: newly-synthesised RNA labelling on isolated peripheral nerve fibres. The capability of dissected myelinated peripheral nerve fibres to synthesise RNA *in vitro* was tested through the incorporation of uridine analogs (5-Bromooxiuridine, BrU) into the newly-synthesised RNA and detected by fluorescent microscopy. Briefly, after preparation of the nerve fibres they were placed immediately in Neurobasal medium containing 2.5 mM BrU (Sigma-Aldrich, MO, USA) and incubated at 37°C and 5% CO_2 for up to 4 hours. BrU is a small compound able to diffuse naturally into the nerve fibres and to incorporate specifically into the newly-transcribed RNA. The presence of newly-transcribed RNA inside the nerve fibres was investigated at three different incubation times (30 min, 2 hours and 4 hours). After incubation, nerve fibres were washed 10 times with fresh medium (without BrU) and fixed with 3% paraformaldehyde for 20 minutes. Finally, newly-synthesised RNA was detected by immunofluorescence using a monoclonal anti-BrdU antibody (concentration 1 : 200, Sigma). Fluorescence images were obtained with confocal microscopy.

Combining AFM and confocal microscopy for mechanical measurements on isolated viable nerve fibres. For mechanical and integrity investigations on myelinated nerve fibres, an integrated AFM and confocal laser scanning microscopy setup was employed. The experimental setup consists of an AFM (Nanowizard® 3 AFM system, JPK instruments, Berlin Germany) coupled to a laser scanning confocal microscope Leica TCS SP8 (Leica, Microsystems, Wetzlar, Germany) equipped with a HC PL Apo 63× oil NA 1.40 lens and 488, 543 and 633 nm lasers lines. The combination of AFM and confocal microscopy allows the investigation of mechanical properties of isolated nerve fibres at the nano-scale level. At the same time it provides fluorescent images showing the extent of nerve fibre compression at a given loading force. Fluorescent transversal sections of myelinated fibres were obtained using an AFM tip-sample delay of approximately 20 seconds. In other words, the AFM tip compressed the fibres at the preset loading force for 20 seconds. This time scale was sufficient to generate confocal fluorescent z-stacks of the fibres while they were being compressed. Special care was taken to precisely position the AFM tip in the centre of nerve fibres in order to avoid undesired compression of the edges. Fluorescent images were acquired with the Leica Application Suite Advanced Fluorescence (LAS AF) software (Leica, Microsystems, Wetzlar, Germany). Confocal images of myelinated nerve fibres were obtained by taking z-stacks of 60 frames with of 0.5 µm spacing at a resolution of 1024 × 16 pixels. The transversal views of myelinated fibres were produced by mounting the z-planes and then rotating them 90° using LAS Montage 3D viewer tool (Leica Microsystems, Wetzlar, Germany). For analytical purposes, during the acquisition of the force-indentation curves used for the elastic Young's modulus calculation the AFM tip-sample delay was set to 0 seconds. The temperature of the sample during the mechanical measurements was controlled and maintained at 37°C using a BioCell™ heater plate (JPK instruments, Berlin, Germany). Three different points along the internodal region (Schwann cell region between two Ranvier nodes) were precisely targeted to perform the mechanical measurements and approximately 5 force-indentation curves were recorded at each point. During data acquisition the tip velocity was set to 1 µm/second.

Studying biomechanical properties of isolated viable nerve fibres: response to mechanical indentation. In the present work, the response of myelinated nerve fibres to mechanical indentation is used as one of the measures for their biomechanical properties. The response of myelinated nerve fibres to indentation was tested with AFM at three increasing loading forces of 25 nN, 50 nN and 75 nN. Briefly, triangular V-shaped MSCT silicon nitride cantilevers (Bruker, CA, USA) with an approximate 0.6 N/m spring constant, 85 µm length and 18 µm width were used to compress the nerve fibres and obtain topographical images. The deflection sensitivity of the cantilever was determined by pushing the probe against a glass coverslip. The portion of the curve in the deflection versus tip-sample distance curve, that represents the physical contact of the AFM tip with the substrate, was used to determine the cantilever sensitivity value. The spring constant of the cantilever was calibrated using the thermal noise method. The utilised cantilever is an irregular pyramid. However, it was considered here as a regular four-sided pyramid for simplicity. The elastic Young's modulus of nerve fibres was determined with the Hertz-Sneddon model corrected for pyramidal indenters[25]. For a sharp-pyramidal AFM tip, the tip-sample force (F) is proportional to the square of the sample indentation (δ), and its relation is given by the following equation:

$$F = \frac{1}{\sqrt{2}} \frac{E \tan \alpha}{(1-\nu^2)} \delta^2$$

F is the loading force, E is the elastic Young's modulus, ν is the Poisson's ratio of the sample (ν = 0.5 is a value commonly used for cells), α is the half-opening angle to the face of the tip (α = 10.7°) and δ is the indentation depth. The Hertz model has some limitations and is generally valid for an indentation depth of 5–10% where the substrate does not influence the calculations. In places we may exceed the valid indentation depth of 10%. Therefore, we clearly consider our calculated values as estimated rather than accurate. We determined an estimated elastic Young's modulus for each genotype due to the fact that the Hertz model is based on simplified assumptions (i.e. isotropic sample, homogeneous elastic surface) that do not describe the mechanical behavior of the peripheral nerve fibres. The estimation of elasticity values corresponding to different structural components within the nerve fibre was based on the analysis of indentation curves and the corresponding confocal images. For the calculation of wild-type and homozygous *Pmp22*$^{-/-}$ nerve fibre elasticity, different portions within the extension curve have been considered. Basically, the extent of nerve fibre deformation applied by the AFM tip to the sample was used to define two different types of elastic measurements named: overall peripheral nerve elasticity (OPN) and basal lamina/Schwann cell myelin elasticity (BL/SCM) as displayed in supplementary figure 3. OPN elasticity is determined by compressing the nerve fibre to a certain extent. In this case, the OPN elasticity is determined by fitting the force-indentation curve from the beginning of the contact point. On the other hand, in order to determine the BL/SCM elasticity as precisely as possible, the axon's internal content is locally largely forced out mechanically. In doing so the contribution of the axon's interior to the BL/SCM elasticity is minimized. Thus, the BL/SCM elasticity is measured following locally compressing the myelinated nerve fibre to such an extent that it is completely squeezed together (see schemes in supplementary figure 3 for explanation). In this case, the BL/SCM elasticity values are determined by fitting the last ~500 nm of the force curve. Curve fitting analysis was carried out using Protein Unfolding and Nano-Indentation Software (PUNIAS, site.voila.fr/punias). Processed data was exported to Origin Pro 8.0 software for graphic production (Origin Lab Corporation, Northampton, MA, USA).

Statistical analysis. Statistical differences in the estimated elastic Young's modulus between wild-type and homozygous *Pmp22*$^{-/-}$ mice were determined by paired Student's t-test. Results are considered statistically different if $p < 0.05$ (indicated by *). Data are given as mean values ± standard error of the mean (SEM).

1. Obremski, V. J., Wood, P. M. & Bunge, M. B. Fibroblasts promote Schwann cell basal lamina deposition and elongation in the absence of neurons in culture. *Dev. Biol.* **160**, 119–134 (1993).
2. Pereira, J. A., Lebrun-Julien, F. & Suter, U. Molecular mechanisms regulating myelination in the peripheral nervous system. *Trends Neurosci.* **35**, 123–134 (2012).
3. Chernousov, M. A., Yu, W. M., Chen, Z. L., Carey, D. J. & Strickland, S. Regulation of Schwann cell function by the extracellular matrix. *Glia* **56**, 1498–1507 (2008).
4. Court, F. A., Wrabetz, L. & Feltri, M. L. Basal lamina: Schwann cells wrap to the rhythm of space-time. *Curr. Opin. Neurobiol.* **16**, 501–507 (2006).
5. Suter, U. & Scherer, S. S. Disease mechanisms in inherited neuropathies. *Nat. Rev. Neurosci.* **4**, 714–726 (2003).
6. Jetten, A. M. & Suter, U. The peripheral myelin protein 22 and epithelial membrane protein family. *Prog. Nucleic Acid Res. Mol. Biol.* **64**, 97–129 (2000).
7. Sancho, S., Young, P. & Suter, U. Regulation of Schwann cell proliferation and apoptosis in PMP22-deficient mice and mouse models of Charcot-Marie-Tooth disease type 1A. *Brain* **124**, 2177–2187 (2001).
8. Amici, S. A., Dunn, W. A., Jr. & Notterpek, L. Developmental abnormalities in the nerves of peripheral myelin protein 22-deficient mice. *J. Neurosci. Res.* **85**, 238–249 (2007).
9. Scherer, S. S. & Wrabetz, L. Molecular mechanisms of inherited demyelinating neuropathies. *Glia* **56**, 1578–1589 (2008).
10. Chance, P. F. *et al.* DNA deletion associated with hereditary neuropathy with liability to pressure palsies. *Cell* **72**, 143–151 (1993).
11. Nicholson, G. A. *et al.* A frame shift mutation in the PMP22 gene in hereditary neuropathy with liability to pressure palsies. *Nat. Genet.* **6**, 263–266 (1994).
12. Li, J., Parker, B., Martyn, C., Natarajan, C. & Guo, J. The PMP22 gene and its related diseases. *Mol. Neurobiol.* **47**, 673–698 (2013).
13. Bai, Y. *et al.* Conduction block in PMP22 deficiency. *J. Neurosci.* **30**, 600–608 (2010).
14. Rosso, G., Negreira, C., Sotelo, J. R. & Kun, A. Myelinating and demyelinating phenotype of Trembler-J mouse (a model of Charcot-Marie-Tooth human disease) analyzed by atomic force microscopy and confocal microscopy. *J. Mol. Recognit.* **25**, 247–255 (2012).
15. Jao, C. Y. & Salic, A. Exploring RNA transcription and turnover in vivo by using click chemistry. *Proc. Natl. Acad. Sci. U. S. A* **105**, 15779–15784 (2008).
16. Adlkofer, K. *et al.* Hypermyelination and demyelinating peripheral neuropathy in Pmp22-deficient mice. *Nat. Genet.* **11**, 274–280 (1995).

17. Adlkofer, K. *et al.* Heterozygous peripheral myelin protein 22-deficient mice are affected by a progressive demyelinating tomaculous neuropathy. *J. Neurosci.* **17**, 4662–4671 (1997).
18. Heredia, A., Bui, C. C., Suter, U., Young, P. & Schaffer, T. E. AFM combines functional and morphological analysis of peripheral myelinated and demyelinated nerve fibers. *Neuroimage.* **37**, 1218–1226 (2007).
19. Huang, W. C., Liao, J. D., Lin, C. C. & Ju, M. S. Depth-sensing nano-indentation on a myelinated axon at various stages. *Nanotechnology.* **22**, 275101 (2011).
20. Liashkovich, I. *et al.* Exceptional mechanical and structural stability of HSV-1 unveiled with fluid atomic force microscopy. *J Cell Sci.* **121**, 2287–2292 (2008).
21. Guo, J. *et al.* Abnormal junctions and permeability of myelin in PMP22-deficient nerves. *Ann. Neurol.* **75**, 255–265 (2014).
22. Amici, S. A. *et al.* Peripheral myelin protein 22 is in complex with alpha6beta4 integrin, and its absence alters the Schwann cell basal lamina. *J. Neurosci.* **26**, 1179–1189 (2006).
23. Hasse, B., Bosse, F., Hanenberg, H. & Muller, H. W. Peripheral myelin protein 22 kDa and protein zero: domain specific trans-interactions. *Mol. Cell Neurosci.* **27**, 370–378 (2004).
24. Monsma, P. C. & Brown, A. FluoroMyelin Red is a bright, photostable and non-toxic fluorescent stain for live imaging of myelin. *J. Neurosci. Methods* **209**, 344–350 (2012).
25. Rico, F. *et al.* Probing mechanical properties of living cells by atomic force microscopy with blunted pyramidal cantilever tips. *Phys. Rev. E. Stat. Nonlin. Soft. Matter Phys.* **72**, 021914 (2005).

Acknowledgments

This study was supported by grants from the German Academic Exchange Service (DAAD), German Research Foundation (Deutsche Forschungsgemeinschaft): SH 167/4-1 and Kosseleck-grant OB63/18, Cells-in-Motion Cluster of Excellence (EXC 1003-CIM), and the International Graduate School GRK1409: "Interaction of pathogens with biotic and abiotic surfaces". We thank Dominik Röhr and Elisabeth Lange for the excellent technical support. We thank Sandra Goebbels (Max Planck Institute for Experimental Medicine, Göttingen) and Ueli Suter (ETH Zürich) for the kind provision of PMP22 knockout mice. We gratefully acknowledge the networking activities of the COST action TD1002.

Author contributions

V.S. designed the experiments, carried out some of them, analysed data and supervised the entire study and wrote up the final version of the paper. G.R. carried out most of the experiments, analysed data, prepared the figures and wrote up a paper draft. I.L. was actively involved in the design and the performing of the experiments as well as in the analysis of the data. B.G. and P.Y. contributed to the design of the experiments and the paper, were actively involved in the analysis of the data and provided essential inputs. A.K. was involved in the design of the experiments and the analysis of the data.

Additional information

Supplementary information accompanies this paper at http://www.nature.com/scientificreports

Competing financial interests: The authors declare no competing financial interests.

How to cite this article: Rosso, G. *et al.* Unravelling crucial biomechanical resilience of myelinated peripheral nerve fibres provided by the Schwann cell basal lamina and PMP22. *Sci. Rep.* **4**, 7286; DOI:10.1038/srep07286 (2014).